Supporting Information

Hybrid Interfacial Layer Leads to Solid Performance Improvement of Inverted Perovskite Solar Cells

Wei Chen,[ab] Yongzhen Wu,[a] Jian Liu,[a] Chuanjiang Qin,[a] Xudong Yang,[a] Ashraful Islam,[a] Yi-Bing Cheng[bc] and Liyuan Han*[ad]

Table S1. Summary on the performance of the reported inverted perovskite solar cells, our solar cells are included for comparison.

Solar Cell Configurations	J_{sc} (mA cm^{-2})	V_{oc} (V)	*FF* (%)	E_{ff} (%)	Reference
ITO/PEDOT/$CH_3NH_3PbI_3$/PCBM/LiF/Al	20.7	0.866	78.3	14.1	*Energy Environ. Sci*., 2014, 7, 2642
ITO/PEDOT/$CH_3NH_3PbI_3$/PCBM/BCP/Al	20.59	0.94	78.8	15.3	*Energy Environ. Sci*., 2014,7, 2619
ITO/PEDOT/PolyTPD/$CH_3NH_3PbI_3$/PCBM/Au	16.12	1.05	67	12.04	*Nature Photonics*, 2014, 8, 128
ITO/PEDOT/CH3NH_3PbI_3/PCBM/Al	10.8	0.91	76	7.4	*Energy Environ. Sci*., 2014, 7, 399
FTO/PEDOT/$CH_3NH_3PbI_{3-x}Cl_x$/PCBM/TiO_x/Al	17.8	1.02	66	11.8	*Nat. Commun.*, 2013, 4, 2761
ITO/PEDOT/$CH_3NH_3PbI_{3-x}Cl_x$/PCBM/Bis-C60/Ag	17.5	0.92	73	11.8	*Adv. Mater*., 2014, 26, 3748
ITO/NiO/meso-NiO/CH3NH3PbI3/BCP/Al	13.24	1.04	69	9.51	*Scientific Reports*, 2014, 4, 4756
ITO/NiO/$CH_3NH_3PbI_{3-x}Cl_x$/PCBM/BCP/Al	12.43	0.92	68	7.8	*Adv. Mater*., 2014, 26, 4107
ITO/NiO/$CH_3NH_3PbI_3$/Al	15.4	1.05	48	7.6	*ACS Photon*., 2014, 1, 547
ITO/sputtered NiO/meso-NiO/$CH_3NH_3PbI_3$/BCP/Al	19.8	0.96	61	11.6	*ACS Appl. Mater. Interfaces*, 2014, 6, 11851
FTO/NiO NCs/$CH_3NH_3PbI_3$/PCBM/Au	16.27	0.882	63.5	9.11	*Angew. Chem.* 2014, DOI: 10.1002/ange.201405176
FTO/NiO/Meso-Al_2O_3/$CH_3NH_3PbI_3$/PCBM/BCP/Ag	16.0	1.05	75	12.7	*This work, perovskite by two step method*
	18.0	1.04	72	13.5	*This work, perovskite by one step method*

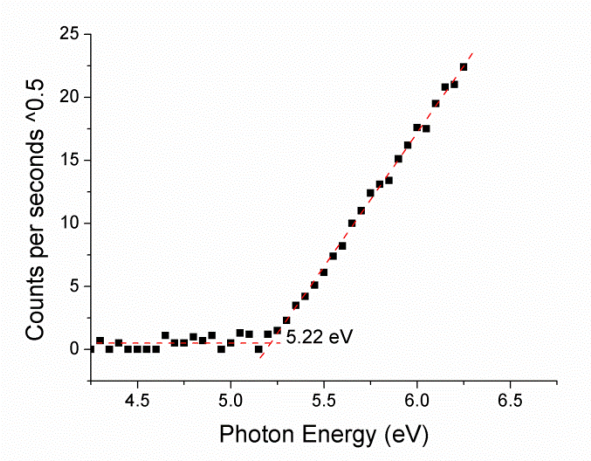

Fig. S1 The ionization potential of NiO compact film tested by the atmospheric photoelectron spectroscopy (AC-3, Riken Keiki Co., Japan).

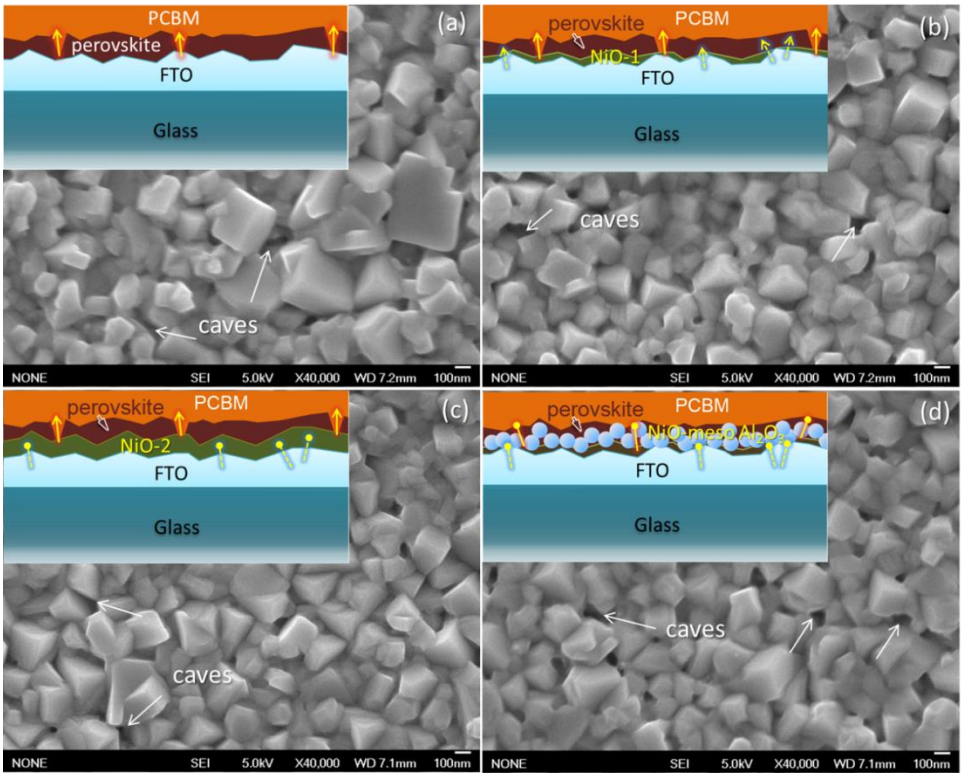

Fig. S2 SEM images of sequential deposited $CH_3NH_3PbI_3$ on different substrates: (a) bare FTO glass, (b) NiO-1 film (thinner film), (c) NiO-2 film (thicker film), and (d) NiO-meso Al_2O_3 combined interfacial layer. The insets depict the possible interfacial current leakage paths (shunt paths) in the four controlled solar cells. The caves between $CH_3NH_3PbI_3$ crystals denoted by the arrows are suggested to play the import roles.

Shunt paths in "Cell bare FTO" as illustrated as the inset in Fig. S2a: FTO/PCBM (PCBM is possibly penetrated through the caves between perovskite crystals denoted by the arrows), due to bare FTO with high conductivity and non-selectivity on charges, the shunt paths between FTO/PCBM are the most detrimental.

Shunt paths in "Cell NiO-1" as illustrated as the inset in Fig. S2b: NiO/PCBM (PCBM is possibly penetrated through the caves between perovskite crystals denoted by the arrows) and/or some uncovered FTO.

Shunt paths in "Cell NiO-2" as illustrated as the inset in Fig. S2c: NiO/PCBM (PCBM is possibly penetrated through the caves between perovskite crystals denoted by the arrows); the shunt paths between uncovered FTO/PCBM will become less (due to better NiO coverage associated with thickness increasing).

Shunt paths in "Cell NiO-meso Al_2O_3" as illustrated as the inset in Fig. S2d: NiO/PCBM shunt paths are strongly blocked, the uncovered FTO will be further blocked due to the coverage of Al_2O_3 nanoparticles.

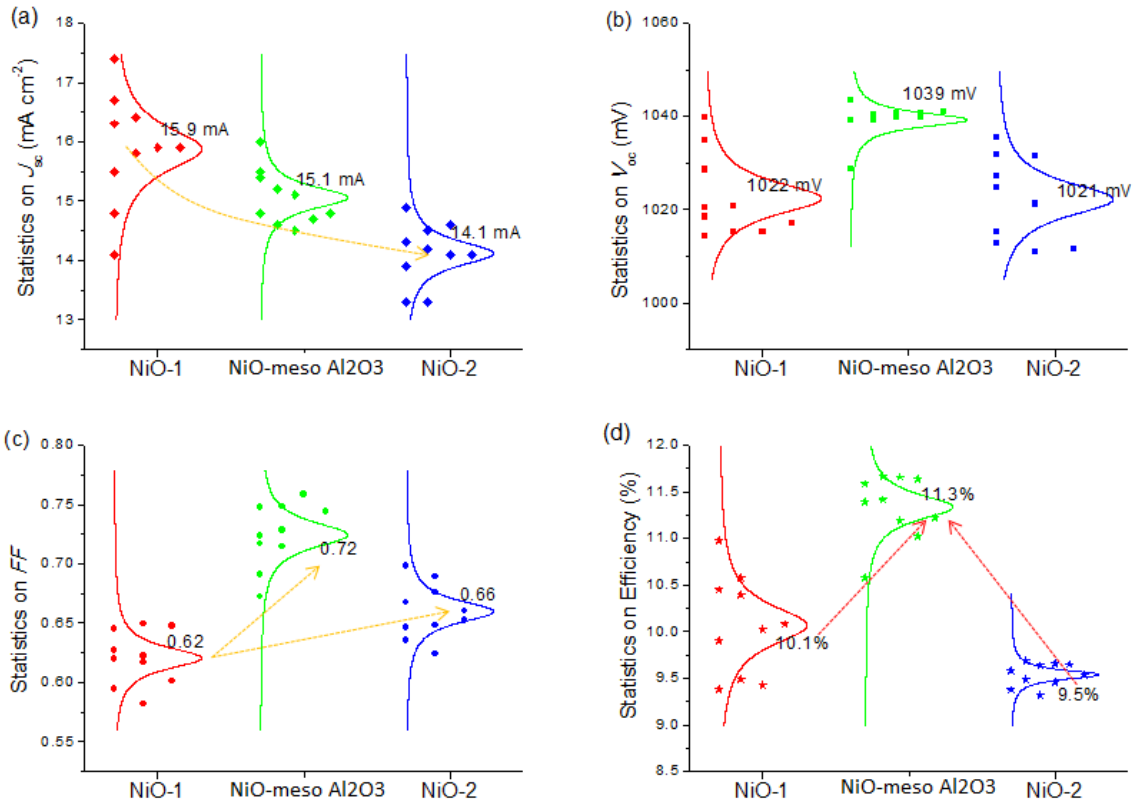

Fig. S3 Statistics on performance parameters of one batch of 10 cells for each of the three compared cell configurations: (a) J_{sc} (b) V_{oc} (c) *FF* (d) efficiency.

These statistics reflect the general variation tendencies of J_{sc}, V_{oc}, *FF* and efficiency dependant on the three compared cell configurations. There are two notable changes: (1) J_{sc} decreases from Cell NiO-1, Cell NiO-meso Al_2O_3, to Cell NiO-2; (2) *FF* increases from Cell NiO-1 to Cell NiO-2, and peaks at Cell NiO-meso Al_2O_3. V_{oc} increases slightly from Cell NiO-1, Cell NiO-2 to Cell NiO-Al_2O_3. In total, efficiency peaks at Cell NiO-meso Al_2O_3. The improvement on efficiency is evident (by 11.9%) due to the additional meso-Al_2O_3 scaffold layer. The reproducibility seems good for our solar cells, which might

be benefit from the facile and controllable solution sequential deposition of perovskite, which makes the films very uniform.

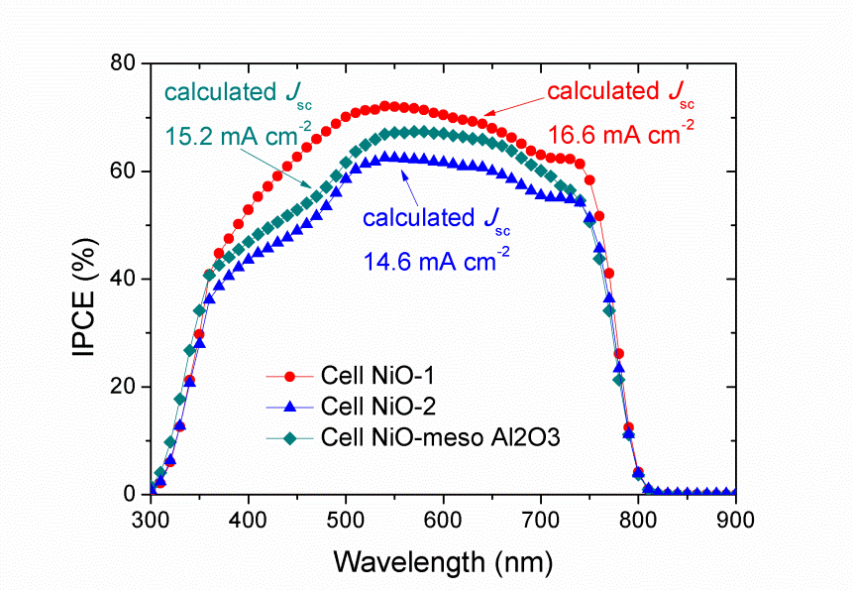

Fig. S4 IPCE spectra of the three compared solar cells in Table 1.

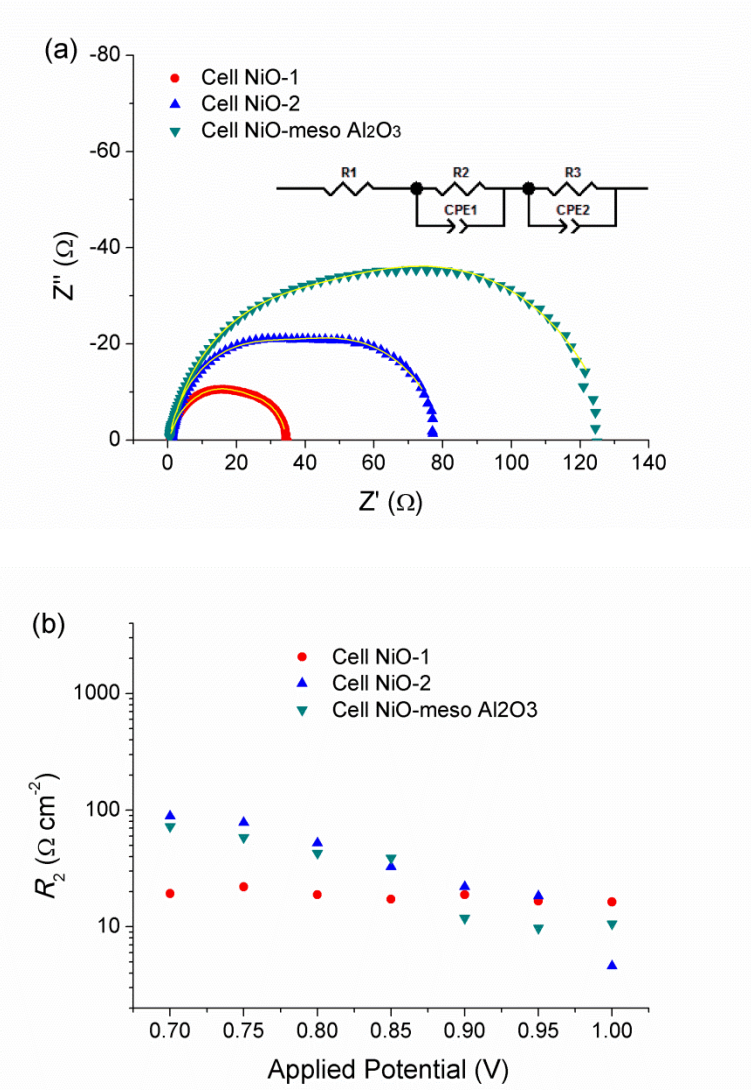

Fig. S5 Nyquist plot of impedance spectra for the tree compared solar cells measured at the bias potential of 0.85 V in the dark, the solid yellow lines are fitted results using the equivalent circuit model shown as the inset; (b) the dependences of fitted resistance (R_2) on different applied bias extracted from the EIS analysis for the three compared solar cells. The changes in R_2 are much smaller in comparison to that of R_3 among the three compared solar cells (as shown in Fig. 3d).

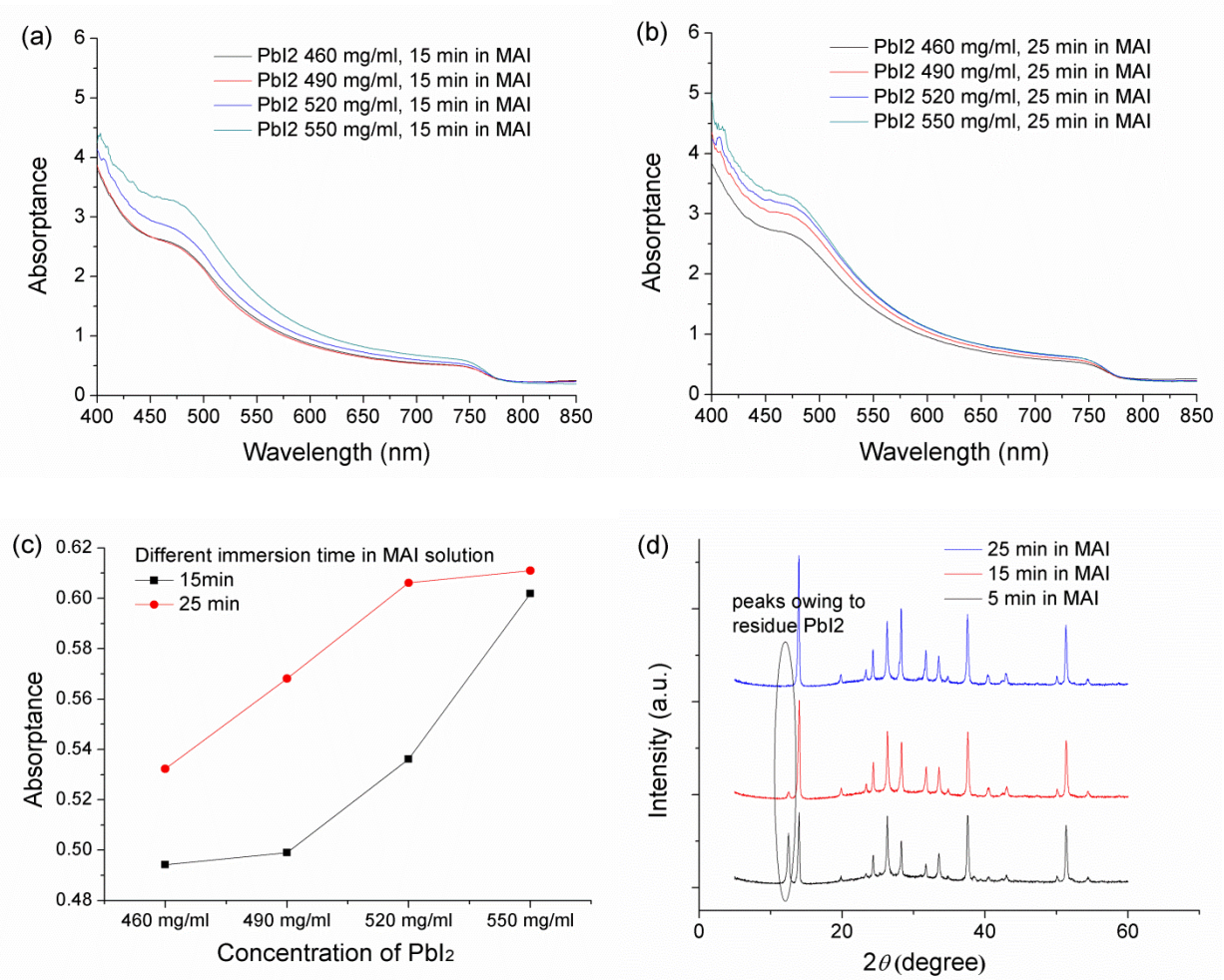

Fig. S6 Light absorptance of a series of perovskite films by spin-coating different concentrations of PbI_2 (460-550 mg/ml in DMF) and immersing in MAI solution for (a) 15 min and (b) 25 min; (c) summary on the light absorptance at 740 nm of the films in (a, b); (d) XRD patterns of the PbI_2 films after immersing in MAI solution for different time.

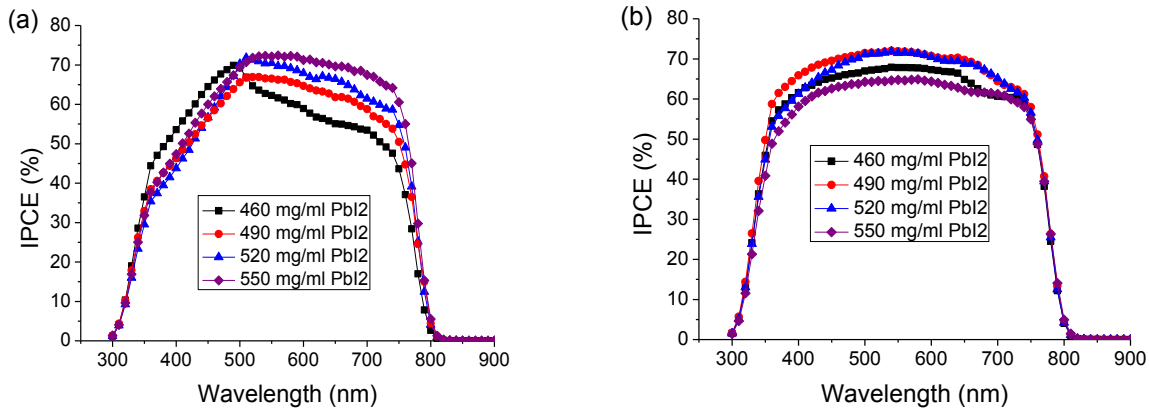

Fig. S7 IPCE spectra of NiO/meso-Al_2O_3 based PSSCs with perovskite layers made by the two-step sequential method, in the first step, spin-coating different concentrations of PbI_2 solutions (460 mg/ml to 550 mg/ml), in the second step, immersing them in MAI solution for (a) 15 min and (b) 25 min.

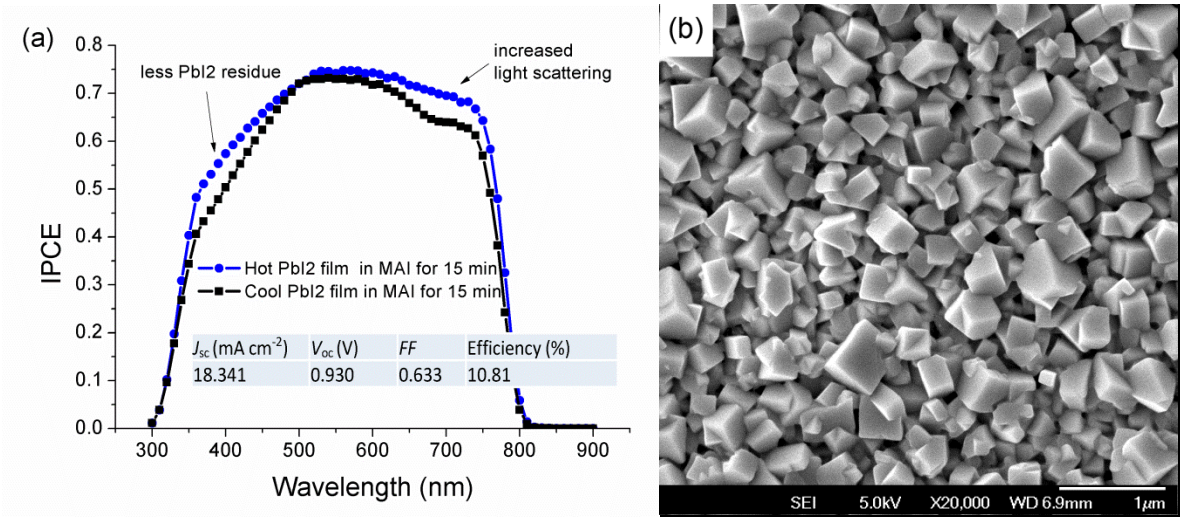

Fig. S8 (a) IPCE spectra of NiO/meso-Al_2O_3 based PSSCs with perovskite layers made by immersing hot or cool PbI_2 film in MAI solution for 15 min, the performance parameters of the hot film based PSSC are shown in the inset table; (b) SEM image of the perovskite film derived from hot PbI_2 film, showing large perovskite crystals.

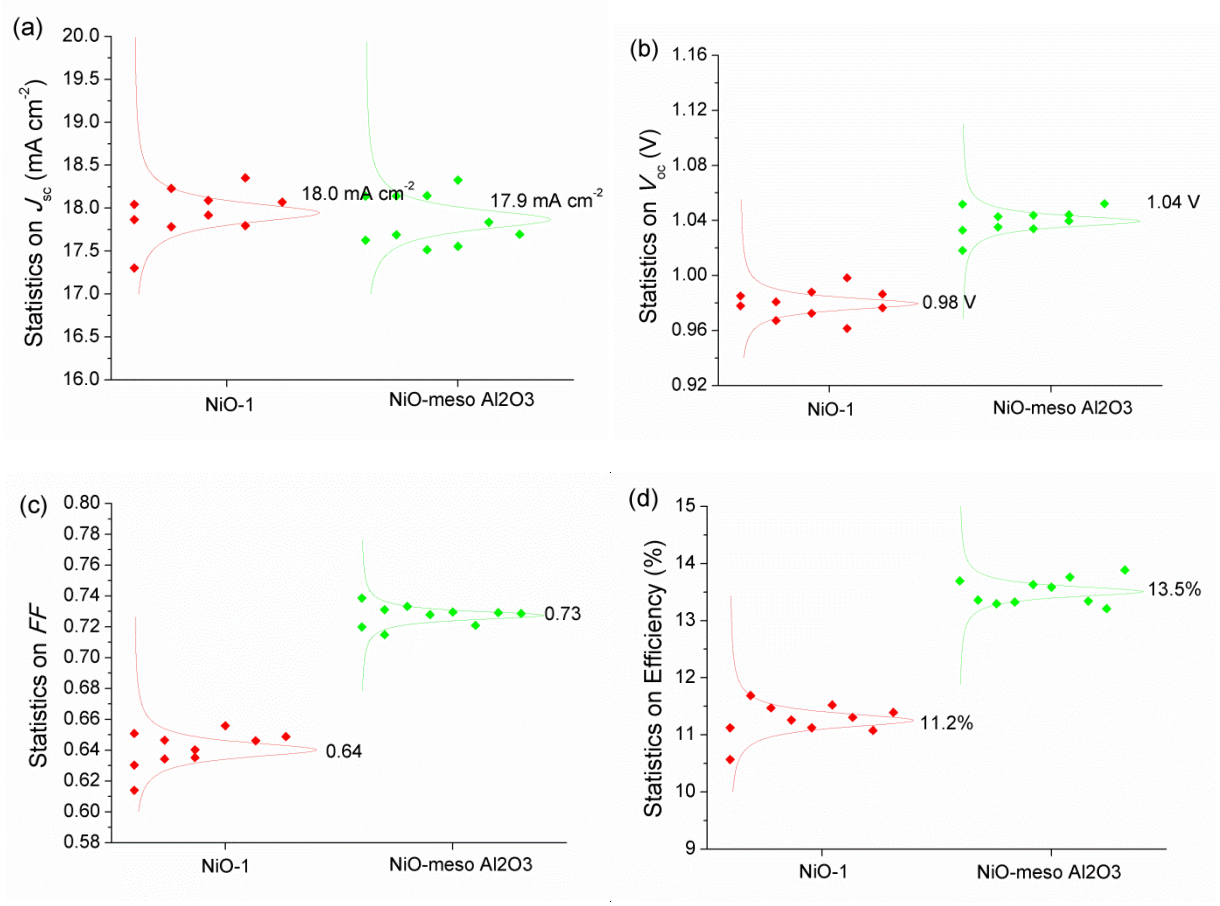

Fig. S9 Statistics on performance parameters of one batch of 10 cells with the planar (NiO-1, "Cell 4" in Table 2) and meso-superstructured (NiO-meso Al_2O_3, "Cell 3" in Table 2) cell configurations: (a) J_{sc} (b) V_{oc} (c) *FF* (d) efficiency. The parameters of NiO-meso Al_2O_3 based solar cells obtained at different scan directions are also compared.

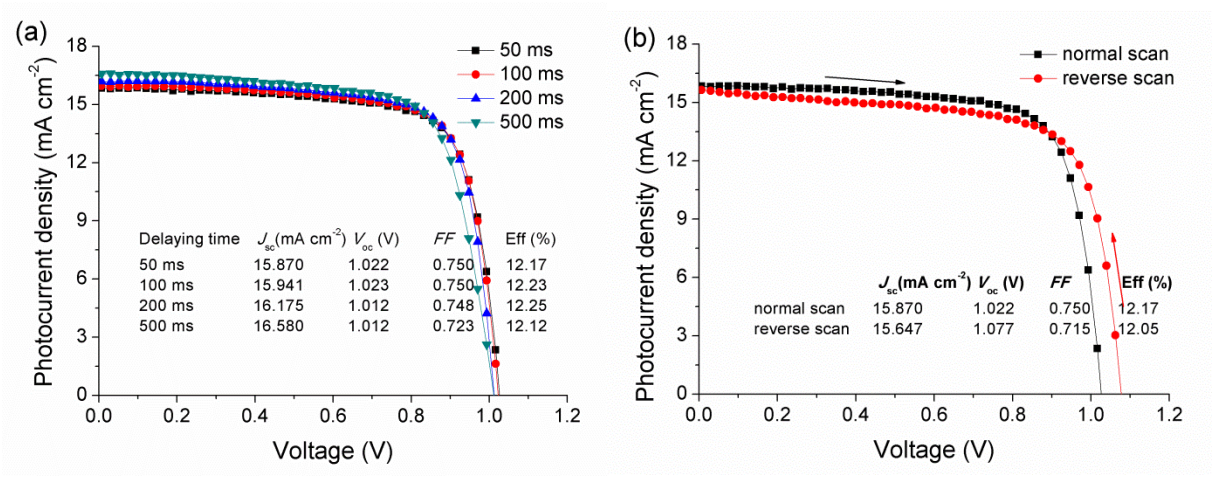

Fig. S10 *J-V* characteristic curves of a cell with the same condition of "Cell 2" (in Table 2) obtained at (a) different scanning rate, with delaying time ranging from 50 ms to 500 ms, (b) different scanning directions.